UDC 621.039

Krar M.E., Badawi M.S., El-Khatib A.M.
Physics Department, Faculty of Science, Alexandria University, 21511 Alexandria, Egypt

USING THE EFFICIENCY TRANSFER METHOD TO CALCULATE THE (FEPE) FOR COMBINATION OF TWO γ-DETECTORS BY USING RADIOACTIVE PARALLELEPIPED SOURCES

The full energy peak efficiency (FEPE) of two γ-detectors by using radioactive parallelepiped sources is computed using a new analytical approach. The approach based on the efficiency transfer method (ET), the effective solid angles and explains the effect of self– absorptions of the source matrix, the attenuation by the source container and the detector housing materials on the detector efficiency. The experimental calibration process was done using radioactive parallelepiped sources containing aqueous 152Eu radionuclide which produces photons with a wide range of energies from 121 up to 1408 keV. The comparison shows a good agreement between the measured and calculated efficiencies for the detector using parallelepiped sources.

Key words: Efficiency Transfer Method (ET), Effective Solid Angle, Full Energy Peak Efficiency (FEPE), Self-Absorptions, Combination of γ-Detectors and Radioactive Parallelepiped Sources.

Introduction

The efficiency, ε , of a gamma-ray detection system is defined in a manner similar to engineering efficiency as a ratio, Eq. 1, where its value tells us how a device (system) is good at detecting the photons originated from the radioactive source.

$$\varepsilon = \frac{\textbf{number of photons recorded by the system}}{\textbf{number of photons emmited by the source}}\Bigg\|_{\textit{in the same time interval}} \quad (1)$$

Unlike engineering efficiency detection efficiency of a system isn't a fixed value assigned to the detection system it's a dynamic value that should assign to each measurement configuration separately as it's dependent on the radioactive source shape, gamma-ray energy, and source to detector geometry as well as any absorber in between the radioactive source and the detection system.

Accurate measurement of detection efficiency plays a central role in the heart of any gamma spectroscopy or quantitative non-destructive elemental analysis; previously the direct mathematical method had been used with high accuracy to calculate efficiencies of cylindrical gamma detectors (Abbas et al. [1-4] ; Hamzawy [5] ; Selim & Abbas [6],[7]), irradiated by different source types and shapes as well as for parallelepiped gamma detectors (Abbas [8],[9]) and also for well-type gamma detectors (Abbas & Selim [10]) , (Abbas [12],[13]), to overcame the sensitivity of the calculated efficiency to frequencies inaccurately reported detector parameters our group recently (El-khatib & Badawi et al. [14] ; Badawi & Abd-Elzaher et al. [15] ; Diab & Badawi et al. [16]). applied the efficiency transfer technique.

Recently, the usage of the multi-detector system has evolved mainly by a contribution from rapid development and widespread of single photon emission computerized tomography (SPECT) and positron emission tomography (PET). In the present work, an extension of the technique to accommodate more than one detector using the bi-detector system using rectangular parallelepiped sources with and without source self-absorption.

Moens et al., 1981 pioneered the efficiency transfer technique. It is based on the proposition that the ratio of the (FEPE) to the effective solid angle is independent of the sample geometry and composition for a given γ-ray energy and is an intrinsic property of the detector (Vidmar & Likar [17]).

The efficiency transfer method (ET), as proposed by Moens and co-authors, is carried out according to the following equation:

$$\varepsilon_{target} = \frac{\Omega_{target}}{\Omega_{ref}} \varepsilon_{ref} \,. \quad (2)$$

Where, ε_{target}, and, ε_{ref} are the (FEPE) for γ-detector using the target [Point, plane and volume] and the reference geometry respectively, while, Ω_{target}, and, Ω_{ref}, are the effective solid angles subtended by the detector surface with the target and the reference geometry respectively. The two effective solid angles were computed by using the direct mathematical method (DMC). The experimental reference efficiency, ε_{ref}, required to use the efficiency transfer technique (Lepy et al. [18]).

Based on the efficiency transfer technique (ET), the present work assumes that: The (FEPF) of a system composed of two discrete detectors using a rectangular radioactive parallelepiped sources can be calculated based on the reference (FEPF) of the system with respect to a radioactive point source as follows.

$$\varepsilon_{rec}^{sys}(E_\gamma) = \frac{\Omega_{rec}^{sys}(E_\gamma)}{\Omega_{ref}^{sys}(E_\gamma)} \varepsilon_{ref}^{sys}(E_\gamma). \quad (3)$$

Where, $\varepsilon_{rec}^{sys}(E_\gamma)$, and, $\varepsilon_{ref}^{sys}(E_\gamma)$, are the (FEPE) for the two combined γ-ray detectors using a rectangular radioactive parallelepiped sources and a radioactive point source as , reference geometry respectively, while, $\Omega_{rec}^{sys}(E_\gamma)$, and, $\Omega_{ref}^{sys}(E_\gamma)$,are the effective solid angles subtended by the detector surface with the target and the reference geometry respectively.

Mathematical Viewpoint

The following sections will explain in details the derivation of the mathematical expressions used to calculate the effective solid angles for using a point aswell as a rectangular parallelepiped sources with respect to a detector in a cylindrical bi-system form. The calculations take into account any present attenuating material in-between the source and the active material of the detection system such as the detector end-cap, holder, and source container material and source self-absorption.

Effective Solid Angle Using Point Source with a Cylindrical Detector

In spherical coordinate system the geometrical solid angle, $\Omega_{Geometrical}$, subtended by a detector surface and an arbitrary located radioactive point source introduced in Pibida et al. [19] and defined as:

$$\Omega_{Geometrical} = \int_\theta \int_\varphi \sin(\theta) d\varphi d\theta. \quad (4)$$

Where, θ, and, φ, are the polar and azimuthal angles respectively, while the effective solid angle, $\Omega_{effective}$,is defined as:

$$\Omega_{effective} = \int_\theta \int_\varphi f_{att} . \sin(\theta) d\varphi d\theta. \quad (5)$$

Where, f_{att}, is a factor to describe the attenuation of the incident radiation due to the different materials acting as attenuators between the source and the detector and can be expressed by the following equation:

$$f_{att} = exp(-\sum_{i=1}^{n} \mu_i . d_i). \quad (6)$$

Where, μ_i, is the total attenuation coefficient, without coherent scattering, of the i^{th} absorber for a γ-ray photon with energy, E_γ, its value obtained from Hubbell & Seltzer [20] ,d_i, is the distance travelled in the material and, n, denotes the number of absorbers between the source and the detector active material.

Considering a cylindrical detector denotes by, Cyl, of radius, R, and depth, L, see figure (1), the effective solid angle, $\Omega_{Pnt}^{Cyl}(h,\rho,R)$, subtended by an arbitrary isotropic point source denotes by ,Pnt, above the detector surface by a distance ,h, and displaced laterally by a distance, ρ, can be rewritten as:

$$\Omega_{pnt}^{Cyl}(h,\rho,R) = \begin{cases} 2\pi \int_0^{\theta_1} f_{att} \sin(\theta) d\theta + 2 \int_{\theta_1}^{\theta_2} \int_0^{\varphi_{max}} f_{att} \sin(\theta) d\theta & \rho < R \\ \\ \int_{\theta_1}^{\theta_2} \int_0^{\varphi_{max}} f_{att} \sin(\theta) d\theta & \rho \geq R \end{cases} \quad (7)$$

While the attenuation factor, f_{att}, can be expressed as the product of the multiplication of two factors as presented on the following equation:

$$f_{att} = f_{hold} f_{cap} \,. \tag{8}$$

Where, f_{hold}, and, f_{cap}, are the attenuation factors due to the holder and the end-cap respectively, each is dependent on both the energy as well as the direction of the emerged photon, while the screening effect of the source as well as the source container were neglected. In addition, the, f_{hold}, can be represented by the following equation:

$$f_{hold} = exp(-\frac{\mu_{hold}.t_{hold}}{\cos(\theta)}) \,. \tag{9}$$

Where, μ_{hold}, is the total linear attenuation coefficient of the holder material and, $t_{hold,}$ is the thickness of the holder and, θ, is the azimuthal angle.

While, $fcap$, can be expressed by the following multi-rang equation, where the representing expression is determined according the values of, θ_1, θ_{cap}, and ϕ_{cap}.

$$f_{cap} = \begin{cases} exp(-\frac{\mu_{cap}.t_{cap}}{\cos(\theta)}) & \theta_1 < \theta_{cap} \\ exp(-\frac{\mu_{cap}.t_{cap}}{\cos(\theta)}) & \phi \le \phi_{cap} \;, \quad \theta_1 > \theta_{cap} \\ exp(-\frac{\mu_{cap}.t_{cap}}{\sin(\theta)}) & \phi > \phi_{cap} \;, \quad \theta_1 > \theta_{cap} \end{cases} \tag{10}$$

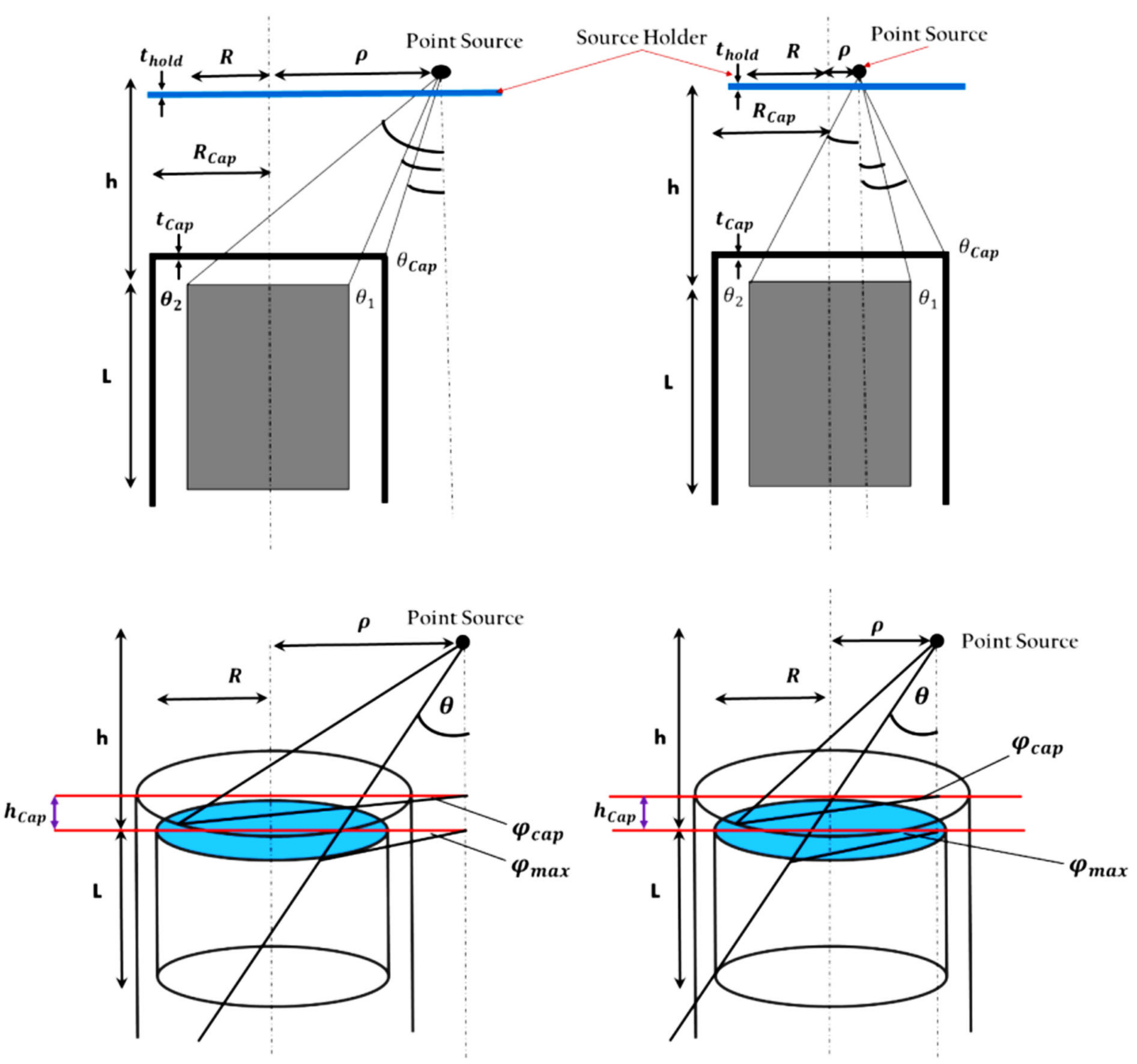

Figure 1 Arbitrary located isotropic point source with cylindrical detector for $\rho \ge$ R and $\rho <$ R

Where, θ, φ, are the polar and azimuthal angles respectively to the direction of the emerged photon; while, μ_{cap}, and, t_{cap},is the total linear attenuation coefficient of the end-cap material and its thickness respectively.

Where the azimuth angle, $\phi_{\max}$, is given by the following equation:

$$\varphi_{\max} = \cos^{-1}\left(\frac{\rho^2 - R^2 + h^2 \tan^2\theta}{2\rho h \tan\theta}\right), \quad (11)$$

and the polar angles are:

$$\theta_1 = \tan^{-1}\left(\frac{|R-\rho|}{h}\right), \quad \theta_2 = \tan^{-1}\left(\frac{R+\rho}{h}\right). \quad (12)$$

Effective Solid Angle Using Point Source with a Bi-Detector

A detection system composed of two discrete active material regions (detectors) here as a bi-detector system. Each region has a cylindrical shape with no restriction on their dimensions, they can also be of a different size from each other, while the separation between the two regions can be arbitrary chosen as described in figure (2).

The separation between the two cylindrical detectors is represented by the axis-to-axis distance D_{12}. R_{D1} and R_{D2} denote the detectors Det-A and Det-B radii respectively, while $L_{D1}$and L_{D2} denotes its lengths. The system arranged such that, the end-caps surfaces of the detectors were placed in the same plane, while the detectors Det-A and Det-B surface was located at Z_{D1} and Z_{D2} under that plane respectively.

The effective solid angle subtended by a radioactive isotropic point source and the surfaces of a system which composed of two detectors (bi-detector) see figure(2) proposed as the sum of the effective solid angles subtended by surfaces of the two cylindrical detectors making up the detection system. The effective solid angle for the system, $\Omega_{pnt}^{Sys}(h, \rho_1, R_1, R_2, D_{12})$, using an isotropic point source located at a distance h from the common end-cap and displaced laterally from the Det-A axis a distance, ρ_1, is expressed as:

$$\Omega_{pnt}^{sys}(h, \rho_1, R_1, R_2, D_{12}) = \\ = \Omega_{pnt}^{A}(h + Z_{D1}, \rho_1, R_1) + \\ + \Omega_{pnt}^{B}(h + Z_{D2}, D_{12} - \rho_1, R_2). \quad (13)$$

Where, $\Omega_{pnt}^{A}(h + Z_{D1}, \rho_1, R_1)$, and $\Omega_{pnt}^{B}(h + Z_{D2}, D_{12} - \rho_1, R_2)$ are the effective solid angles subtended by the surface of the detector Det-A and Det-B from the point source, respectively.

Effective Solid Angle Using Rectangular Parallelepiped with a Bi-Detector

Consider a rectangular parallelepiped source, see figure (3), its width denoted as, W_S, while its depth denoted as, D_S, and its height denoted as ,L_S. The source placed arbitrary how-

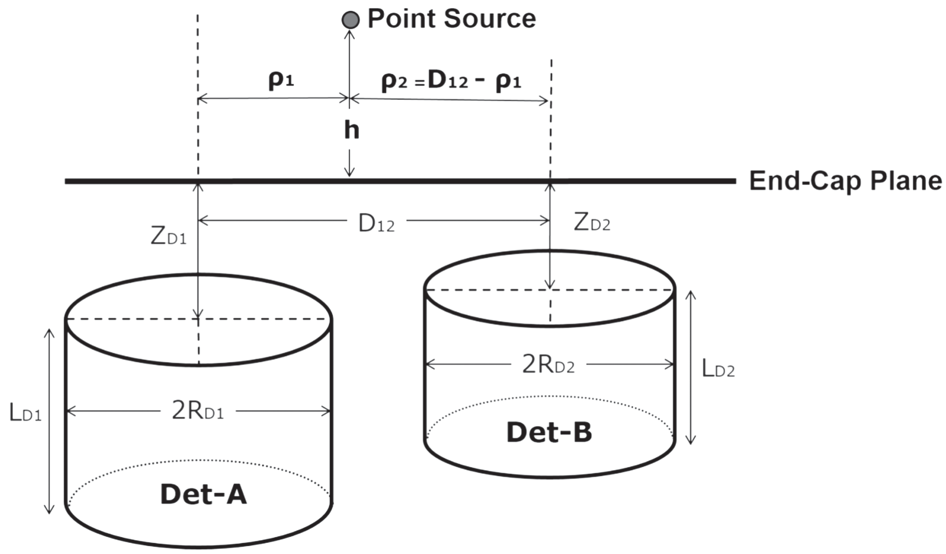

Figure (2) Schematic diagram describes the bi-detector system with an arbitrary point source.

ever, its plane of symmetry is coincident with the plane of symmetry of the detection system. The source separated from the common end-cap is denoted by H_S, and its axis is laterally from Det-A is denoted, X_S.

Previously (Hamzawy, [5]) had treated a volumetric radioactive source as a group of point sources that are uniformly distributed. Similarly, using appropriate Cartesian coordinate system, the effective solid angle of the volumetric rectangular parallelepiped source, $^{sys}_{rec}(W_S, D_S, L_S, X_S, H_S, Z_D)$, can be expressed by the following integration:

$$\Omega^{sys}_{rec}(W_S, D_S, L_S, X_S, H_S) = \frac{2\int\limits_{H_s}^{H_s+L_s}\int\limits_{0}^{D_s/2}\int\limits_{-W_S/2}^{W_S/2}\Omega^{sys}_{pnt}(x,y,z)\,dxdydz}{V}. \quad (14)$$

Where the integrand, $^{sys}_{pnt}(x, y, z)$, represents the effective solid angle of the system surface subtended by a point source located at Cartesian coordinate, (x,y,z), as in Fig.3 and represented by the following equation:

$$\Omega^{sys}_{pnt}(x,y,z) = \\ = \Omega^{A}_{pnt}(Z_{D1} + H_S + z, \rho_1, R_1) + \\ + \Omega^{B}_{pnt}(Z_{D2} + H_S + z, D_{12} - \rho_2, R_2). \quad (15)$$

Where the lateral distances can be expressed in the Cartesian coordinate system by the following equations:

$$\rho_1 = \sqrt{(x_s + x)^2 + (y)^2}, \\ \rho_2 = \sqrt{(x_s - x)^2 + (y)^2}. \quad (16)$$

Where, f_{att}, in equation (6) represent the attenuation due to the source self absorption and the other absorbers between the source and the detector where it can be given following equation:

$$f_{att} = f_s\, f_{con}\, f_{hold}\, f_{cap}. \quad (17)$$

Where, f_s, f_{con}, f_{hold}, and f_{cap}, represent the attenuation due to the source, source container material, holder and end-cap respectively, each is dependent on both the energy as well as the direction of the emerged photon.

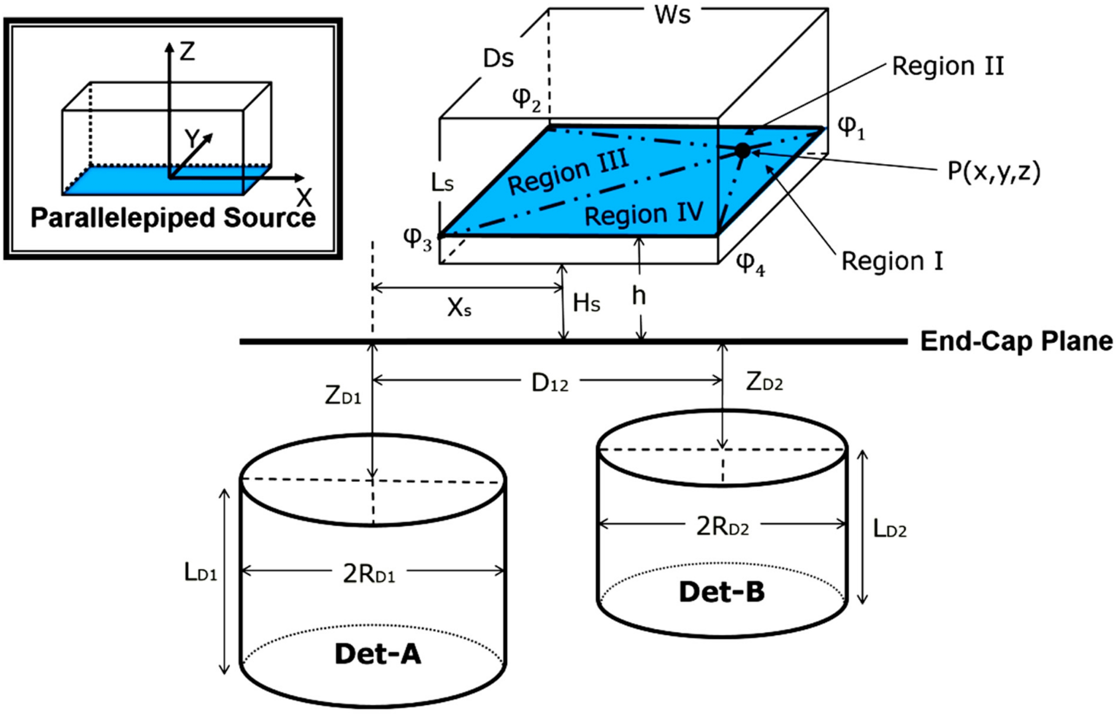

Figure (3) Schematic diagram describes the bi-detector detection system with an arbitrary located parallelepiped source

The attenuation due to holder material, f_{hold}, can be represented by the following equation:

$$f_{hold} = exp(-\frac{\mu_{hold}.t_{hold}}{\cos(\theta)}). \qquad (18)$$

Where, μ_{hold}, is the total linear attenuation coefficient of the holder material and, t_{hold}, is the thickness of the holder material and θ is the polar angle.

While, f_{cap}, can be expressed by the following multi-rang equations, where the expression representing it, according to the values of, θ, θ_{cap}, and, ϕ_{cap}.

$$f_{cap} = \begin{cases} exp(-\frac{\mu_{cap}.t_{cap}}{\cos(\theta)}) & \theta_1 < \theta_{cap} \\ exp(-\frac{\mu_{cap}.t_{cap}}{\cos(\theta)}) & \phi \le \phi_{cap}, \theta_1 > \theta_{cap} \\ exp(-\frac{\mu_{cap}.t_{cap}}{\sin(\theta)}) & \phi > \phi_{cap}, \theta_1 > \theta_{cap} \end{cases} \qquad (19)$$

Where, θ, and, φ, are the polar and azimuthal angles respectively to the direction of the emerged photon; while, μ_{cap}, and , t_{cap}, is the total linear attenuation coefficient of the end-cap material and its thickness respectively.

The polar angle, θ_{cap}, is given by the following equation:

$$\theta_{cap} = \tan^{-1}\left(\frac{|R_{cap} - \rho|}{h - h_{cap}}\right). \qquad (20)$$

While the azimuthal angle, φ_{cap}, is given by the following equation:

$$\varphi_{cap} = \cos^{-1}\left(\frac{\rho^2 - (R_{cap})^2 + (h - h_{cap})^2 \tan^2\theta}{2\rho(h - h_{cap})\tan\theta}\right) \qquad (21)$$

Where, R_{cap}, and, h_{cap}, are the end-cap radius and its surface separation from the detector surface respectively.

In addition, the mathematical expression for, f_s, and, f_{con}, presented in table (1) the azimuthal angle, φ, divided into four regions as depicted in figure (3) bounded by the azimuthal angles stated by the following equations:

$$\phi_1 = \tan^{-1}\left(\frac{\frac{1}{2}D_s - y}{\frac{1}{2}W_s - x}\right),$$

$$\phi_2 = \tan^{-1}\left(\frac{\frac{1}{2}D_s - y}{\frac{1}{2}W_s + x}\right),$$

$$\phi_3 = \tan^{-1}\left(\frac{\frac{1}{2}D_s + y}{\frac{1}{2}W_s + x}\right),$$

$$\phi_4 = \tan^{-1}\left(\frac{\frac{1}{2}D_s + y}{\frac{1}{2}W_s - x}\right). \qquad (22)$$

Where, μ_s, and , μ_{con}, are the total linear attenuation coefficient without the coherent scattering for the source matrix and container material respectively, while, t_{con}, is the container thickness and the parameters, $\alpha^{\pm}$, and , $\beta^{\pm}$, are given by the following equations.

$$\alpha^{\pm} = \frac{\frac{1}{2}W_s \pm x}{\cos(\phi)}, \quad \beta^{\pm} = \frac{\frac{1}{2}D_s \pm y}{\sin(\phi)}. \qquad (23)$$

Accordingly the (FEPF) of a system composed of two detectors using a rectangular radioactive parallelepiped sources given by equation (2) and equation (12) and (13) can be calculated based on the reference (FEPF) of the system with respect to a radioactive point source as follows.

$$\varepsilon_{rec}^{sys}(E_\gamma) = \frac{\Omega_{rec}^{sys}(W_S, D_S, L_S, X_S, H_S)}{\Omega_{pnt}^{sys}(h, \rho_1, R_1, R_2, D_{12})}\varepsilon_{pnt}^{sys}(E_\gamma). \qquad (24)$$

Experimental Setup

Experimental measurements were done using a set of standard point sources obtained from PTB, Germany and a set of a rectangular homemade radioactive parallelepiped sources in different volumes. The certificates show the sources activities and their uncertainties are listed in table (2) and table (3). The data sheet states the values of half-life photon energies and photon emission probabilities per decay for all radionuclides used in the calibration process are listed in table (4), which is available at the National Nuclear Data Center Web Page or on the IAEA website.

The detection system composed of two cylindrical NaI (Tl) scintillation detectors (Model 802 scintillation detectors– Canberra) of differ-

Table (1) Mathematical description of the self-absorption and container factors.

Regions	Self-absorption factor (f_s)	Container attenuation factor (f_{con})
Region I ($0 \le \varphi < \varphi_1$ or $\varphi_4 < \varphi < 2\pi$)	$\begin{cases} exp(-\frac{\mu_s.z}{\cos(\theta)}) & \theta \le \tan^{-1}\left(\frac{\alpha^-}{z}\right) \\ exp(-\frac{\mu_s.(\frac{1}{2}W_s - x)}{\sin(\theta)}) & \theta > \tan^{-1}\left(\frac{\alpha^-}{z}\right) \end{cases}$	$\begin{cases} exp(-\frac{\mu_{con}.t_{con}}{\cos(\theta)}) & \theta \le \tan^{-1}\left(\frac{\alpha^-}{z}\right) \\ exp(-\frac{\mu_{con}.t_{con}}{\sin(\theta)}) & \theta > \tan^{-1}\left(\frac{\alpha^-}{z}\right) \end{cases}$
Region II ($\varphi_1 \le \varphi < \varphi_2$)	$\begin{cases} exp(-\frac{\mu_s.z}{\cos(\theta)}) & \theta \le \tan^{-1}\left(\frac{\beta^-}{z}\right) \\ exp(-\frac{\mu_s.(\frac{1}{2}D_s - y)}{\sin(\theta)}) & \theta > \tan^{-1}\left(\frac{\beta^-}{z}\right) \end{cases}$	$\begin{cases} exp(-\frac{\mu_{con}.t_{con}}{\cos(\theta)}) & \theta \le \tan^{-1}\left(\frac{\beta^-}{z}\right) \\ exp(-\frac{\mu_{con}.t_{con}}{\sin(\theta)}) & \theta > \tan^{-1}\left(\frac{\beta^-}{z}\right) \end{cases}$
Region III ($\varphi_2 \le \varphi < \varphi_3$)	$\begin{cases} exp(-\frac{\mu_s.z}{\cos(\theta)}) & \theta \le \tan^{-1}\left(\frac{\alpha^+}{z}\right) \\ exp(-\frac{\mu_s.(\frac{1}{2}W_s + x)}{\sin(\theta)}) & \theta > \tan^{-1}\left(\frac{\alpha^+}{z}\right) \end{cases}$	$\begin{cases} exp(-\frac{\mu_{con}.t_{con}}{\cos(\theta)}) & \theta \le \tan^{-1}\left(\frac{\alpha^+}{z}\right) \\ exp(-\frac{\mu_{con}.t_{con}}{\sin(\theta)}) & \theta > \tan^{-1}\left(\frac{\alpha^+}{z}\right) \end{cases}$
Region IV ($\varphi_3 \le \varphi < \varphi_4$)	$\begin{cases} exp(-\frac{\mu_s.z}{\cos(\theta)}) & \theta \le \tan^{-1}\left(\frac{\beta^+}{z}\right) \\ exp(-\frac{\mu_s.(\frac{1}{2}D_s + y)}{\sin(\theta)}) & \theta > \tan^{-1}\left(\frac{\beta^+}{z}\right) \end{cases}$	$\begin{cases} exp(-\frac{\mu_{con}.t_{con}}{\cos(\theta)}) & \theta \le \tan^{-1}\left(\frac{\beta^+}{z}\right) \\ exp(-\frac{\mu_{con}.t_{con}}{\sin(\theta)}) & \theta > \tan^{-1}\left(\frac{\beta^+}{z}\right) \end{cases}$

Table (2) PTB point sources activities and their uncertainties

PTB-Nuclide	Activity (KBq)	Reference Date 00:00 Hr	Uncertainty
^{152}**Eu**	290.0	1.June 2009	± 1.38%
^{137}**Cs**	385.0		± 0.71%
^{60}**Co**	212.1		± 1.04%

Table (3) Characteristic of the rectangular parallelepiped sources

Standard Source					Container	
ID	**Length**	**Width**	**Height**	**Volume**	**Material**	**Thickness**
V1	5.9 cm	3.8 cm	5.2 cm	100 mL	HDPE	0.15 cm
V2	6.1 cm	6.1 cm	6.2 cm	200 mL	PP	0.15 cm
Both have activity (5 KBq ± 1.98%, Reference date January 1st ,2010)						

ent sizes 3”x 3” [Det-A, figure(4-A)] and 2”x 2” [Det-B, figure (4-B)]. The detectors mounted vertically in a specially constructed holder figure (4-C) made of Teflon such that the distance from side end-cap to side end-cap by 1 cm. The details of these detectors setup parameters with acquisition electronics specifications supported by the serial and model number are listed in table (5).

The measurements were done using radioactive sources placed at 30 cm above the detector common end-cap which allows to minimize the dead time and to neglect the effect of coincidence summing on the experimental results, while all lateral distances are reported relative to the axis of symmetry of Det-A.

The ^{152}Eu point source and homemade rectangular radioactive parallelepiped sources V1 and V2 were used to establish the experimental calibration curves, in order to be compared with those calculated by the present work. Besides that, two standard point sources ^{60}Co and ^{137}Cs used for energy calibration, as well as gain adjust to make matching between the channels while acquisition in both detectors done.

The measurements were carried out to obtain statistically significant main peaks in the spectra that are recorded and processed by win-TMCA32 software made by ICx Technologies. Measured spectrum was saved as spectrum ORTEC files which can be opened by ISO 9001 Genie 2000 data acquisition and analysis software made by Canberra where the peak analysis accomplished. The acquisition time is high enough to get at least the number of counts 20,000, which make the statistical uncertainties less than 0.5%. Typical acquisition time for a point source was several hours but for volumetric sources not less than 48 hours for each measurement according to low activity. The spectra are analyzed with the program using its automatic peak search and peak area calculations, along with changes in the peak fit using the interactive peak fit interface when necessary to reduce the residuals and error in the peak area values. The peak areas, the live time, the run time and the start time for each spectrum are entered in the spreadsheets that are used to perform the calculations necessary to generate the efficiency curves.

Table 4. Half-life, photon energies and photon emission probabilities per decay for all radionuclides used in this work

PTB-Nuclide	Energy (Kev)	Emission Probability, %	Half Life (Days)
^{152}Eu	121.78	28.4	4943.29
	244.69	7.49	
	344.28	26.6	
	778.9	12.96	
	964.13	14.0	
	1408.01	20.87	
^{137}Cs	661.66	85.21	11004.98
^{60}Co	1173.23	99.9	1925.31
	1332.5	99.982	

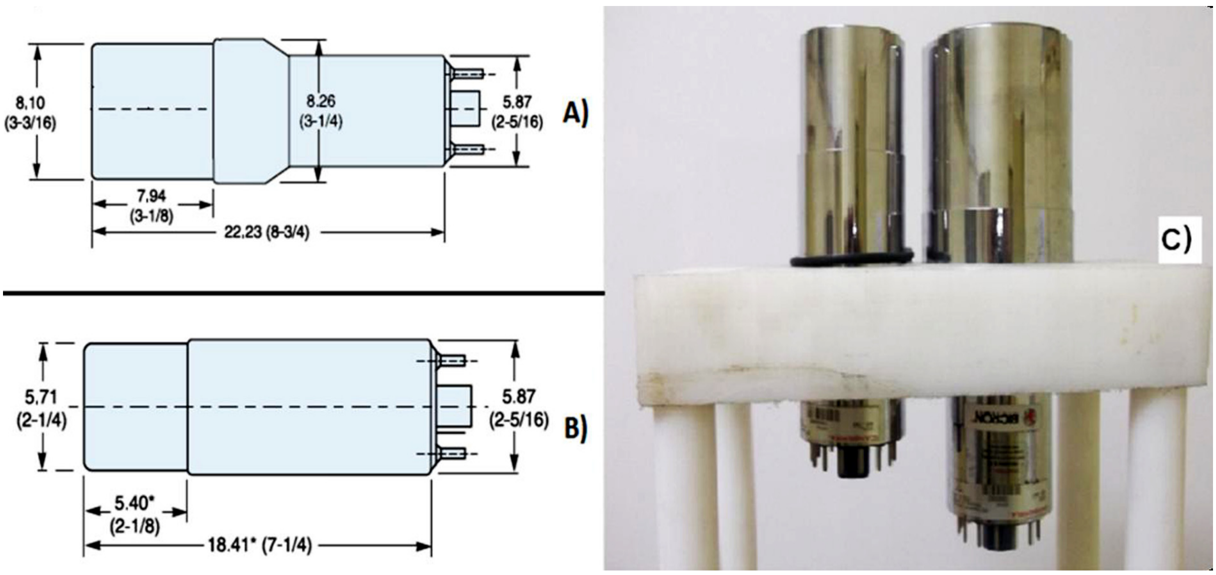

Figure 4. A) 3”x 3” detector dimension in cm (inch), B) 2”x 2” detector dimension in cm (inch) and C) mounting of the bi-detector system in a specially designed holder

Results and Discussion

The measured efficiency values as a function of the photon energy, $\varepsilon(E)$, for both NaI(Tl) Scintillation detectors were calculated using the following formula:

$$\varepsilon(E) = \frac{N(E)}{T \cdot A_s \cdot P(E)} \prod C_i . \qquad (25)$$

Where, N(E), is the number of counts in the full-energy peak and it was obtained using Genie 2000 software, T, is the measuring time (in second), P(E),is the photon emission probability at energy, E, was obtained from Genie 2000 standard library while, A_S, is the radionuclide activity and, C_i, represents the correction factors due to dead time and radionuclide decay.

No summing correction was done due to the low dead time associated with measurements and the corresponding correction factor for the dead time was obtained simply using (ADC) live time. However, the background subtraction was done which was extremely important for low activity rectangular sources. The decay correction, C_d, for the calibration source from the reference time to the run time was given by:

$$C_d = \exp(\lambda \cdot \Delta T). \qquad (26)$$

Where, λ, is the decay constant and, ΔT, is the time interval over which the source allowed to decay until the run time. The main source of uncertainty in the efficiency calculations was the uncertainties of the activities of the standard source solutions. The uncertainty in the (FEPE), σ_ε, was given by:

$$\sigma_\varepsilon = \varepsilon \cdot \sqrt{\left(\frac{\sigma_N}{\partial N}\right)^2 + \left(\frac{\sigma_A}{\partial A}\right)^2 + \left(\frac{\sigma_P}{\partial P}\right)^2} . \qquad (27)$$

Where, σ_N, σ_A, σ_P, is the uncertainties associated with the uncertainties in the quantities, N(E), A_S, and , P(E), respectively.

The percentage deviations between the calculated (with and without self-absorption) and the measured full-energy peak efficiency values are calculated by:

$$\Delta_1\% = \frac{\varepsilon_{\text{cal-with self}} - \varepsilon_{\text{meas}}}{\varepsilon_{\text{cal-with self}}} \times 100 , \qquad (28)$$

$$\Delta_2\% = \frac{\varepsilon_{\text{cal-without self}} - \varepsilon_{\text{meas}}}{\varepsilon_{\text{cal-without self}}} \times 100 , \qquad (29)$$

where, $\varepsilon_{\text{cal-with self}}$, $\varepsilon_{\text{cal-without self}}$, and, $\varepsilon_{\text{meas}}$, are the calculated with / without self-absorption factor

Table 5. Detectors setup parameters with acquisition electronics specifications for Detector (Det-A) and Detector (Det-B)

Items	Detector (Det-A)	Detector (Det-B)
Manufacturer	Canberra	Canberra
Serial Number	09L 652	09L 654
Detector Model	802	802
Type	Cylindrical	Cylindrical
Mounting	Vertical	Vertical
Resolution (FWHM) at 661 keV	8.5%	7.5%
Cathode to Anode voltage	+1100 V dc	+1100 V dc
Dynode to Dynode	+80 V dc	+80 V dc
Cathode to Dynode	+150 V dc	+150 V dc
Tube Base	Model 2007	Model 2007
Shaping Mode	Gaussian	Gaussian
Detector Type	NaI(Tl)	NaI(Tl)
Crystal Diameter (mm)	76.2	50.8
Crystal Length (mm)	76.2	50.8
Top cover Thickness (mm)	Al (0.5)	Al (0.5)
Side cover Thickness (mm)	Al (0.5)	Al (0.5)
Reflector – Oxide (mm)	2.5	2.5
Weight (Kg)	1.8	0.77
Outer Diameter (mm)	80.9	57.2
Outer Length (mm)	79.4	53.9
Crystal Volume in (cm^3)	347.639	103.004

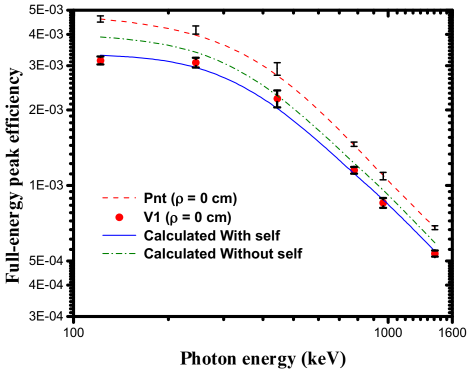

Figure 5 The calculated full-energy efficiency values(with and without self-absorption) and the measured ones with their associated uncertainties as a function of the photon energy for bi-detector using (V1) mounted axial to Det-A while its centers elevated 30 cm above the common end-cap plane and a point-like source at the (V1) center

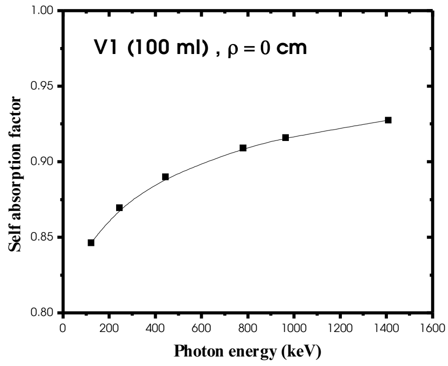

Figure 6 The self absorption factor calculated as a function of the photon energy for bi-detector using (V1) mounted axial to Det-A while its centers elevated 30 cm above the common end-cap plane

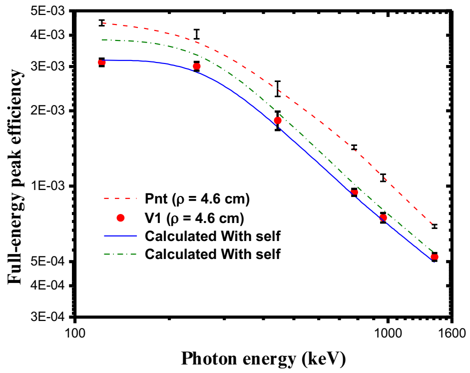

Figure 7 The calculated full-energy efficiency values(with and without self-absorption) and the measured ones with their associated uncertainties as a function of the photon energy for bi-detector using (V1) mounted 4.6 cm lateral to Det-A while its centers elevated 30 cm above the common end-cap plane and a point-like source at the (V1) center

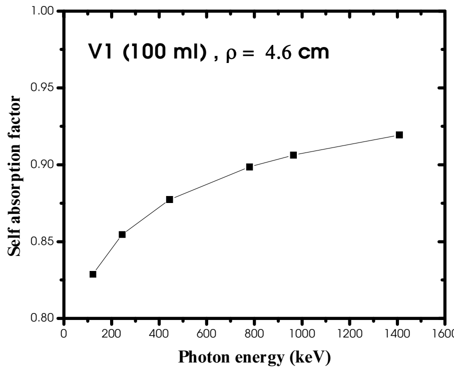

Figure 8 The self absorption factor calculated as a function of the photon energy for bi-detector using (V1) mounted 4.6 cm lateral to Det-A while its centers elevated 30 cm above the common end-cap plane

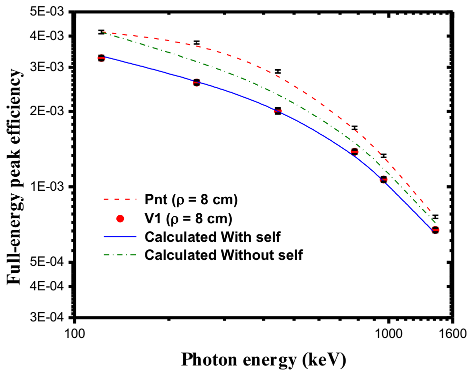

Figure 9 The calculated full-energy efficiency values(with and without self-absorption) and the measured ones with their associated uncertainties as a function of the photon energy for bi-detector using (V1) mounted axial to Det-B while its centers elevated 30 cm above the common end-cap plane and a point-like source at the (V1) center

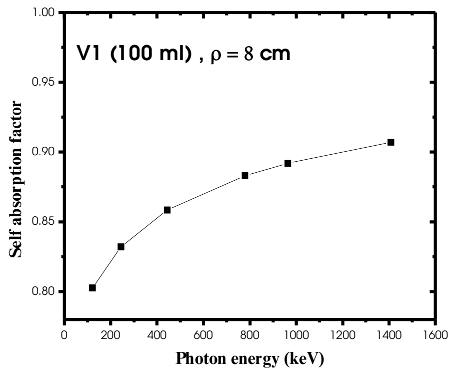

Figure 10 The self absorption factor calculated as a function of the photon energy for bi-detector using (V1) mounted axial to Det-B while its centers elevated 30 cm above the common end-cap plane

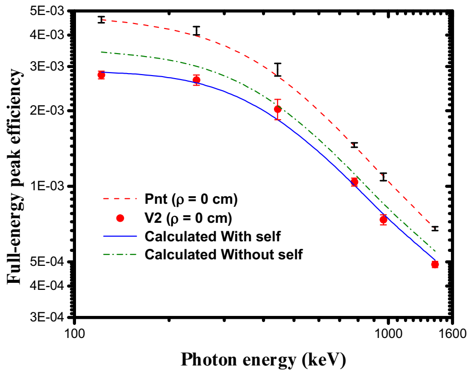

Figure 11 The calculated full-energy efficiency values (with and without self-absorption) and the measured ones with their associated uncertainties as a function of the photon energy for bi-detector using (V2) mounted axial to Det-A while its centers elevated 30 cm above the common end-cap plane and a point-like source at the (V2) center

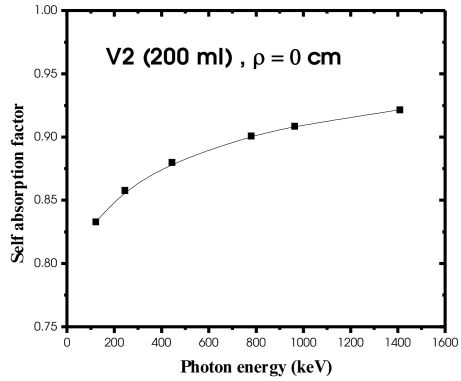

Figure 12 The self absorption factor calculated as a function of the photon energy for bi-detector using (V2) mounted axial to Det-A while its centers elevated 30 cm above the common end-cap plane

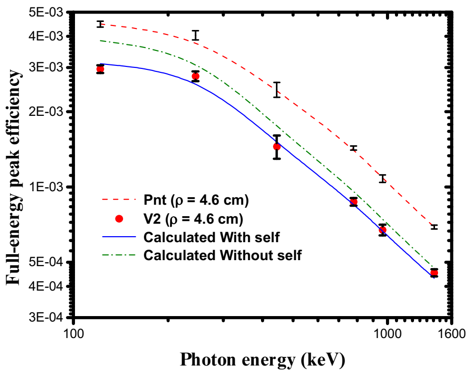

Figure 13 The calculated full-energy efficiency values (with and without self-absorption) and the measured ones with their associated uncertainties as a function of the photon energy for bi-detector using (V2) mounted 4.6 cm lateral to Det-A while its centers elevated 30 cm above the common end-cap plane and a point-like source at the (V2) center

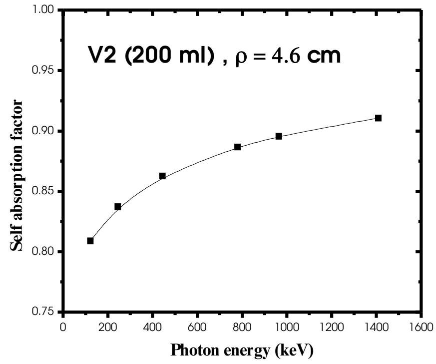

Figure 14 The self absorption factor calculated as a function of the photon energy for bi-detector using (V2) mounted 4.6 cm lateral to Det-A while its centers elevated 30 cm above the common end-cap plane

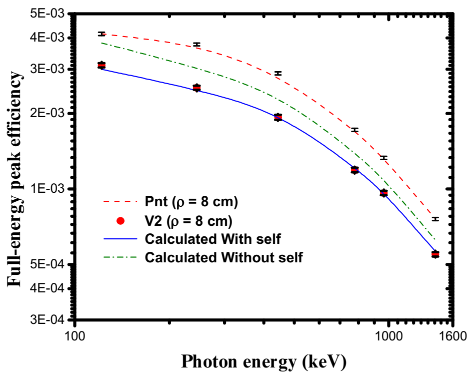

Figure 15 The calculated full-energy efficiency values (with and without self-absorption) and the measured ones with their associated uncertainties as a function of the photon energy for bi-detector using (V2) mounted 8 cm lateral to Det-B while its centers elevated 30 cm above the common end-cap plane and a point-like source at the (V2) center

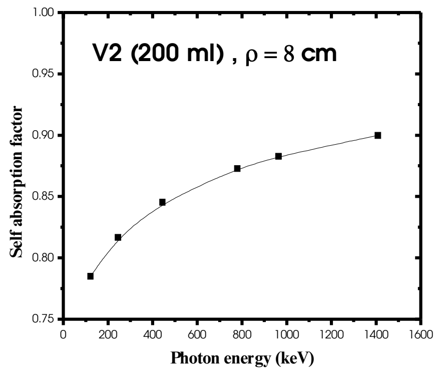

Figure 16 The self absorption factor calculated as a function of the photon energy for bi-detector using (V2) mounted axial to Det-B while its centers elevated 30 cm above the common end-cap plane and experimentally measured efficiencies, respectively.

All the integrals encountered are elliptic integrals and does not have a closed form solution, so a numerical solution is obtained using the trapezoidal rule. Although the accuracy of the integration increases with increasing the number of intervals n, the integration converges well at n=20. A computer program (using Microsoft QuickBasic Program) has been written to calculate the effective solid angles for arbitrary located point as well as volumetric sources based on the derived equations.

The deviation of the measured (FEPE) and the calculated efficiencies based on equation (24) of the two γ-detector system with their associated uncertainties as a function of the photon energy using the two volumetric rectangular parallelepiped sources (V1 and V2) are depicted in the (Figure.5, 7,9,11, 13 and 15) respectively. These volumetric sources produced energy range from 121 keV up to 1408 keV and placed such that: its center elevated 30 cm from the system common end-cap and has a lateral displacement 0 cm, 4.6 cm and 8 cm. According to table. (1), the self attenuation factor is depending on two main factors which are the absorption coefficient of the source matrix and the path length through the source itself. The effect of these factors can be shown in (Figure.6, 8, 10, 12, 14 and 16) which represents the variation of the self absorption factor obtained with the photon energy. The self absorption factor for 100 mL is greater than that of 200 mL when the two sources are placed at the same position with respect to the two γ-detector system; this is because the path length calculated for 100 mL is smaller than that for 200 mL, So as the parallelepiped source volume increases, the importance of the self absorption factor becomes noteworthy and can't be neglected in the detector calibration, but must be calculated with more accuracy to obtain good results. Also, the self-absorption factor increases by increasing the energy, and that is related to the effect of the absorption coefficient of the source matrix. Table 6, 7 and 8 shows the comparison between the percentage deviations Δ_1% and Δ_2% for different volumes (V1 & V2) placed at its center at 30 cm from the system common end-cap and has a lateral displacement 0 cm, 4.6 cm and 8 cm.

Table 6. The discrepancies between the measured and the calculated (FEPE) with (Δ_1%) and without (Δ_2%) self-absorption using (V1 and V2) while axial to Det-A

Energy (keV)	Volume (V1=100 mL)		Volume (V2=200 mL)	
	Δ 1%	Δ 2%	Δ 1%	Δ 2%
121.78	5.08	24.16	2.52	23.07
244.69	1.62	16.87	2.64	19.65
443.98	-4.05	7.82	-3.94	9.16
778.89	-3.48	6.19	-1.92	8.86
964.01	3.99	13.55	3.94	14.40
1407.95	2.24	10.24	4.10	12.96

Table 7. The discrepancies between the measured and the calculated (FEPE) with (Δ_1%) and without (Δ_2%) self-absorption using (V1 and V2) while placing 4.6 cm lateral to Det-A axis of symmetry

Energy (keV)	Volume (V1=100 mL)		Volume (V2=200 mL)	
	Δ 1%	Δ 2%	Δ 1%	Δ 2%
121.78	1.92	22.97	5.07	29.88
244.69	50.32	23.24	2.89	22.88
443.98	-4.37	9.00	3.45	19.91
778.89	-3.60	7.28	-1.03	19.91
964.01	-2.67	7.39	-1.63	9.83
1407.95	-4.98	3.35	-5.07	4.25

Table 8. The discrepancies between the measured and the calculated (FEPE) with (Δ_1%) and without (Δ_2%) self-absorption using (V1 and V2) while axial to Det-B

Energy (keV)	Volume (V1=100 mL)		Volume (V2=200 mL)	
	Δ 1%	Δ 2%	Δ 1%	Δ 2%
121.78	1.83	26.86	-3.54	22.90
244.69	1.92	22.47	-1.58	20.51
443.98	2.99	19.97	5.18	24.41
778.89	-2.17	10.78	2.52	17.47
964.01	-0.93	11.06	0.83	14.23
1407.95	-3.13	6.79	2.55	13.98

Conclusion

In this work, a new analytical approach based on the efficiency transfer method for the calculation of the full-energy peak efficiency (FEPE) of a combination of two γ-detectors using point and parallelepiped sources has been deduced. In addition, the authors introduced separate calculation of the factors related to photon attenuation in the detector end cap, dead layer, source container and the self-attenuation of the source matrix. In addition, the self-attenuation coefficient of the source matrix was calculated and its influence appears when we are dealing with large sources, or with small photon energies. According to the results, there is a good agreement between the calculated (with source self-absorption correction) and the measured full-energy peak efficiencies using ^{152}Eu aqueous radioactive source placed in parallelepiped beakers with different volumes. The percentage deviation between them is less than 6%. Therefore, the present work can be successfully applied to the efficiency calibration of a combination of two γ-detectors with high accuracy.

12.05.2013

Acknowledgments

The authors would like to express their sincere thanks to Prof. Dr. Mahmoud. I. Abbas, Faculty of Science, Alexandria University for his fruitful scientific collaborations on this topic also the authors would like to introduce a special thanks to The Physikalisch-Technische Bundesanstalt (PTB) in Braunschweig, Berlin, Germany for fruitful help in preparing the homemade volumetric sources.

References
[1] Y. S. Selim and M. I. Abbas, «Direct Calculation of the Total Efficiency of Cylindrical Scintillation Detectors for Extended Circular Sources,» *Radiat. Phys. Chem.*, 48 (1996) 23.
[2] Y. S. Selim and M. I. Abbas, «Analytical calculations of gamma scintillators effi ciencies II . Total efficiency for wide coaxial circular disk sources,» *Radiat. Phys. Chem.*, vol. 58 (2000) 15.
[3] M. I. Abbas, «HPGe detector photopeak efficiency calculation including self-absorption and coincidence corrections for Marinelli beaker sources using compact analytical expressions.,» Appl. Radiat. Isot., 54 (2001) 761.
[4] M. I. Abbas, S. Nafee, and Y. S. Selim, «Calibration of cylindrical detectors using a simplified theoretical approach.,» Appl. Radiat. Isot., 64 (2006) 1057.
[5] M. I. Abbas, «Direct mathematical method for calculating full-energy peak efficiency and coincidence corrections of HPGe detectors for extended sources,» Nucl. Instrum. Methods Phys. Res. B, vol. 256, no. 1, pp. 554–557, Mar. 2007.
[6] A. Hamzawy, «Validation of analytical formula for the efficiency calibration of gamma detectors using coaxial and off-axis extended sources,» Nucl. Instrum. Methods Phys. Res. A, 618(2010) 216.
[7] M. I. Abbas, Y. S. Selim, and M. Bassiouni, «HPGe detector photopeak efficiency calculation including self-absorption and coincidence corrections for cylindrical sources using compact analytical expressions,» *Radiation Physics and Chemistry*,61 (2001) 429.
[8] M. I. Abbas, «A direct mathematical method to calculate the efficiencies of a parallelepiped detector for an arbitrarily positioned point source,» *Radiation Physics and Chemistry*, 60 (2001) 3.
[9] M. I. Abbas, «Validation of analytical formulae for the efficiency calibration of gamma detectors used in laboratory and in-situ measurements.,» Appl. Radiat. Isot., 64 (2006) 1661.
[10] M. I. Abbas, «Analytical formulae for well-type NaI (Tl) and HPGe detectors efficiency computation.,» Appl. Radiat. Isot., 55 (2001) 245.
[11] M. I. Abbas and Y. S. Selim, «Calculation of relative full-energy peak efficiencies of well-type detectors,» Nucl. Instrum. Methods Phys. Res. A, 480 (2002) 651.
[12] M. I. Abbas, «Analytical calculations of the solid angles subtended by a well-type detector at point and extended circular sources.,» Appl. Radiat. Isot., *industry and medicine*, 64 (2006) 1048.
[13] M. I. Abbas, «Analytical approach to calculate the efficiency of 4π NaI(Tl) gamma-ray detectors for extended sources,» Nucl. Instrum. Methods Phys. Res. A, 615 (2010) 48.
[14] A. M. El-khatib, M. S. Badawi, M. A. Elzaher, and A. A. Thabet, «New Analytical Approach to Calculate the Full Energy Peak Efficiency for NaI (Tl) Gamma-Ray Detector Using the Effective Solid Angle Method,» *International Journal of Instrumentation Science*, 1 (2012) 25.
[15] M. S. Badawi, M. Abd-Elzaher, A. A. Thabet, A. M. El-khatib, «An empirical formula to calculate the full energy peak efficiency of scintillation detectors» Appl. Radiat. Isot. 74 (2013) 46.
[16] S. M. Diab, M. S. Badawi, A. M. El-khatib, S. S. Nafee, and E. A. El-, «Computation of the Efficiency of NaI (Tl) Detectors Using Radioactive Inverted Well Beaker Sources Based on Efficiency Transfer Technique,» *Journal of Advanced Research in Physics*, 4 (2013) 1.
[17] T. Vidmar and A. Likar, «On the invariability of the total-to-peak ratio in gamma-ray spectrometry.,» Appl. Radiat. Isot. 60 (2004) 191.
[18] M. C. Lepy, T. Altzitzoglou, et al. «Intercomparison of efficiency transfer software for gamma-ray spectrometry.,» Appl. Radiat. Isot. 55 (2001) 493.
[19] L. Pibida, S. S. Nafee, M. Unterweger, M. M. Hammond, L. Karam, and M. I. Abbas, «Calibration of HPGe gamma-ray detectors for measurement of radioactive noble gas sources.,» Appl. Radiat. Isot. 65 (2007) 225.
[20] J. H. Hubbell and S. M. Seltzer, «Tables of X-ray mass attenuation coefficients and mass energy-absorption coefficients 1 keV to 20 MeV for elements Z=1 to 92 and 48 additional substances of dosimetric interest,» *NISTIR-5632 USA.*, vol. 5632, 1995.

M. E. Krar, Physics Department, Faculty of Science, Alexandria University, 21511 Alexandria, Egypt.
[Assistance Lecturer], e-mail: drkrar@gmail.com, Tel:+201113398479.
M. S. Badawi, Physics Department, Faculty of Science, Alexandria University, 21511 Alexandria, Egypt.
[Doctor], e-mail: ms241178@hotmail.com, Tel:+201005154976.
A. M. El-Khatib, Physics Department, Faculty of Science, Alexandria University, 21511 Alexandria, Egypt.
[Professor. Doctor], e-mail: Elkhatib60@yahoo.com, Tel:+201000230122.